

Journal of Biomedical Optics

BiomedicalOptics.SPIEDigitalLibrary.org

Platform to investigate aqueous outflow system structure and pressure-dependent motion using high-resolution spectral domain optical coherence tomography

Sepideh Hariri
Murray Johnstone
Yi Jiang
Steven Padilla
Zhehai Zhou
Roberto Reif
Ruikang K. Wang

Platform to investigate aqueous outflow system structure and pressure-dependent motion using high-resolution spectral domain optical coherence tomography

Sepideh Hariri,^a Murray Johnstone,^b Yi Jiang,^b Steven Padilla,^b Zhehai Zhou,^{a,c} Roberto Reif,^a and Ruikang K. Wang^{a,b,*}

^aUniversity of Washington, Department of Bioengineering, Seattle, Washington 98195, United States

^bUniversity of Washington, Department of Ophthalmology, Seattle, Washington 98195, United States

^cBeijing Information Science and Technology University, Beijing Laboratory of Biomedical Detection Technology and Instruments, Beijing 100192, China

Abstract. The aqueous outflow system (AOS) is responsible for maintaining normal intraocular pressure (IOP) in the eye. Structures of the AOS have an active role in regulating IOP in healthy eyes and these structures become abnormal in the eyes with glaucoma. We describe a newly developed system platform to obtain high-resolution images of the AOS structures. By incorporating spectral domain optical coherence tomography (SD-OCT), the platform allows us to systematically control, image, and quantitate the responses of AOS tissue to pressure with a millisecond resolution of pulsed flow. We use SD-OCT to image radial limbal segments from the surface of the trabecular meshwork (TM) with a spatial resolution of $\sim 5 \mu\text{m}$ in *ex vivo* nonhuman primate eyes. We carefully insert a cannula into Schlemm's canal (SC) to control both pressures and flow rates. The experimental results demonstrate the capability of the platform to visualize the unprecedented details of AOS tissue components comparable to that delivered by scanning electron microscopy, as well as to delineate the complex pressure-dependent relationships among the TM, structures within the SC, and collector channel ostia. The described technique provides a new means to characterize the anatomic and pressure-dependent relationships of SC structures, particularly the active motion of collagenous elements at collector channel ostia; such relationships have not previously been amenable to study. Experimental findings suggest that continuing improvements in the OCT imaging of the AOS may provide both insights into the glaucoma enigma and improvements in its management. © The Authors. Published by SPIE under a Creative Commons Attribution 3.0 Unported License. Distribution or reproduction of this work in whole or in part requires full attribution of the original publication, including its DOI. [DOI: [10.1117/1.JBO.19.10.106013](https://doi.org/10.1117/1.JBO.19.10.106013)]

Keywords: optical coherence tomography; glaucoma; aqueous outflow system; trabecular meshwork; Schlemm's canal; dynamic motion.

Paper 140526R received Aug. 19, 2014; revised manuscript received Sep. 24, 2014; accepted for publication Sep. 25, 2014; published online Oct. 28, 2014.

1 Introduction

Glaucoma is the second leading cause of blindness worldwide and elevated intraocular pressure (IOP) is the only treatable risk factor in glaucoma.¹ Elevated IOP is caused by a loss of the ability of aqueous to flow from the anterior chamber (AC) through the structures of aqueous outflow system (AOS), a premise established by the classic studies of Grant.^{2,3} Structures through which aqueous passes include trabecular meshwork (TM), Schlemm's canal (SC), and collector channel ostia (CCO) along the external scleral wall of SC that are the entrances to collector channels.⁴ From the intrascleral collector channels, aqueous flows through the sclera to conjunctival vessels on the surface of the eye.

Two studies recently documented that SC is a lymphatic-like vessel⁵ acquiring a lymphatic identity with lymphatic valve markers such as Fox2c as well as cell junctions and basement membrane properties similar to collecting lymphatics.⁶ The latter study references evidence^{7,8} that oscillatory aqueous pulse waves originating in SC might explain the presence of SC

Fox2c expression, an expression profile that requires tissue within SC to experience ongoing oscillatory shear stress. It is well accepted that lymphatics provide remarkably tight control of short-term interstitial pressure homeostasis in tissues as well as lymphatic fluid movement through pulse-dependent oscillatory vessel wall motion.⁹ Intrinsic mechanotransduction mechanisms that control lymphatic vessel wall mechanics provide long-term homeostasis. Such generalizable concepts of vessel wall motion as a means of maintaining fluid pressure homeostasis⁹ may also be an important factor in homeostatic control of aqueous movement through SC; these considerations emphasize the value of developing imaging techniques to study the motion of SC tissues.

Recently, a series of minimally invasive glaucoma surgeries (MIGS) have been developed to reduce IOP. The goal of these procedures and devices is to provide a means of direct aqueous passage through the TM into SC, ideally at the entrances of CCO.^{10,11} Strides in the development of MIGS have provided a compelling need to develop improved AOS imaging techniques for several purposes: (1) to better understand their mechanism of action, (2) to image CCO to optimize device placement, (3) to design devices that bridge and prevent damage

*Address all correspondence to: Ruikang K. Wang, E-mail: wangrk@uw.edu

to CCO, and (4) to better understand why bypassing the TM, which provides direct aqueous access to SC and CCO, typically only achieves pressure lowering to the mid-teens.¹⁰ In addition, the current limitations of MIGS to lower IOP also emphasize the need to identify resistant factors present in SC and at CCO along the SC external wall.

Optical coherence tomography (OCT) provides high-resolution ($<10\ \mu\text{m}$) and high-speed imaging of three-dimensional (3-D) tissue structures and permits dynamic noninvasive real-time assessments of living tissue.¹²⁻¹⁴ These attributes make OCT a valuable tool for studying the AOS in normal and glaucoma eyes. OCT is, in fact, currently being explored to investigate the AOS in animal^{15,16} and human eyes.¹⁷⁻²⁵

Several OCT studies have shown the correlation between cross-sectional SC area and IOP, consistent with previous findings of pressure-dependent movement in *ex vivo* human and nonhuman primate (NHP) eyes using a morphometric analysis system.²⁶ For example, the SC area has been shown to decrease in response to acute change in IOP in healthy human subjects.²⁷ Furthermore, it has been shown that the SC area is significantly smaller in glaucomatous compared to normal eyes.^{25,28} In addition to responses to applied chronic pressure, the trabecular tissues have been shown by phase sensitive OCT to respond to rapid ocular transients, such as cyclic motion induced by the ocular/cardiac pulse both in *ex vivo* primate¹⁶ and *in vivo* human eyes.¹⁹

Although these efforts have provided useful information, OCT imaging to quantify SC dimensions and characterize the time scale of TM motion remains challenging. Both scattering from the limbal tissue and shadowing from the vasculature above SC reduce the effective power of the imaging beam reaching the canal. These two factors are responsible for diminished image contrast, making it difficult to visualize and accurately delineate the borders of SC, which additionally precludes the characterization of structures within the canal.²⁸ Longer wavelengths may be used to enhance light penetration into the tissue, leading to improved image contrast but at the expense of reduced axial resolution.²⁴ A recently developed AC approach using an endoscopic OCT probe to image the AOS from the TM surface circumvents the scattering and shadowing problems, permitting identification of CCO.²⁹ However, the reported probe only allows for an imaging rate of 0.5 frames per second (fps), limiting its usefulness in characterizing the AOS. The limitation is particularly apparent when there is a requirement to image the dynamic responses of tissue components to cyclic pulse-induced variations of IOP.

Motion artifacts are inevitable for *in vivo* studies, which make comparative studies problematic because it is difficult to repeatedly image the same location. A particularly difficult additional challenge arises from the fact that in *ex vivo* as well as *in vivo* NHP and human eyes, the SC lumen is little more than a potential space with the TM in close approximation to the CCO area.^{26,30} The relationships of structures spanning between the TM and CCO cannot be easily studied nor their motion easily characterized.

To address these challenges, we describe a newly developed experimental setup that enables imaging of the outflow system from the TM surface in *ex vivo* NHP eyes using a high-resolution spectral domain OCT (SD-OCT). To accommodate the proposed setup for imaging AOS, we specifically designed the SD-OCT system with a short working distance in the sample arm, allowing for improved imaging resolution and contrast suitable for high-speed visualization of the fine structure and

movement of the TM and resultant changes in SC lumen dimensions. In addition, the system was designed for direct access from TM surface side, which is important because it avoids light attenuation by the surrounding tissue.

In the proposed setup, a cannula is inserted into SC that leads to either constant pressure reservoirs or a perfusion pump. Constant pressures dilate SC, revealing AOS structural elements. Alternatively, the perfusion pump can be used to introduce pulse transients to permit assessment of AOS motion. Our purpose is twofold: (1) to determine whether the experimental design allows high-resolution SD-OCT to provide quantitative assessment of the TM, SC, and CCO structures and (2) to determine whether rapid the pressure-dependent motion of AOS structures can be imaged and quantified.

2 Materials and Methods

2.1 System Setup

The experimental setup used in this study [Fig. 1(a)] is composed of a perfusion system that can infuse fluid into the SC lumen in radial limbal segments while being imaged by an OCT system. The OCT is an SD-OCT design that utilizes a broadband superluminescent diode with a 110-nm spectral bandwidth centered at 1340 nm to achieve a theoretical axial resolution of $\sim 7.2\ \mu\text{m}$ in air. A spectrometer with a 0.14-nm spectral resolution and an InGaAs line scan camera with 1024 pixels capable of $\sim 92\ \text{KHz}$ A-line rate was used to provide a measured axial imaging range of $\sim 3\ \text{mm}$ in air. The dynamic range of 105 dB was measured at a depth of 0.5 mm for a 2.5-mW incident sample beam power. An 18-mm objective lens was used in the sample arm to focus the beam at the corneo-scleral limbus region, resulting in a lateral resolution of $\sim 10\ \mu\text{m}$ measured by $1/e^2$ beam size at the focus.

We developed an SC insertion cannula that was steeply tapered and flexible, a crucial factor in the imaging protocol. We noticed that if the cannula was made of rigid glass with a standard pipette puller, it would be too narrow to occlude the SC entrance. In addition, the rigid glass cannulas also tend to cut the trabecular tissues rather than sliding along the contour of the canal lumen. Accordingly, Polyethylene 60 tubing (Instech Laboratories Inc., Plymouth Meeting, Pennsylvania) was used in this study to make the appropriate cannulas to serve our purpose. To make the cannula, a length of Polyethylene tubing was rotated in an arc while being held $\sim 1\ \text{mm}$ from the end of a fine tip soldering iron (Apex Hand Tools-WSB25HK). The tubing was gently pulled until the central portion achieved an approximate outside diameter (OD) smaller than the desired size. To properly size the cannula tip, the tubing was placed next to a slide micrometer and cut at the appropriate OD with a razor blade knife. The cannulas selected for use had an approximate length of taper of 4.5 mm and an outside tip cannula diameter of 130 to 150 μm . Selection of the optimized cannula taper resulted in a rejection rate of $\sim 95\%$.

AOS tissue consisting of radial limbal segments [Fig. 1(b)] is mounted with pins in a Petri dish with the TM surface facing the imaging probe [Fig. 1(c)]. Assisted by an optical microscope and a micromanipulator, a cannula with a 150 to 200 μm OD is carefully inserted into the SC lumen. The other end of the cannula is connected to a perfusion system. Valves permit switching between a Harvard Perfusion PumpTM and a reservoir at a height that generates a defined pressure. Alternatively, the setup can switch between two reservoirs at different heights

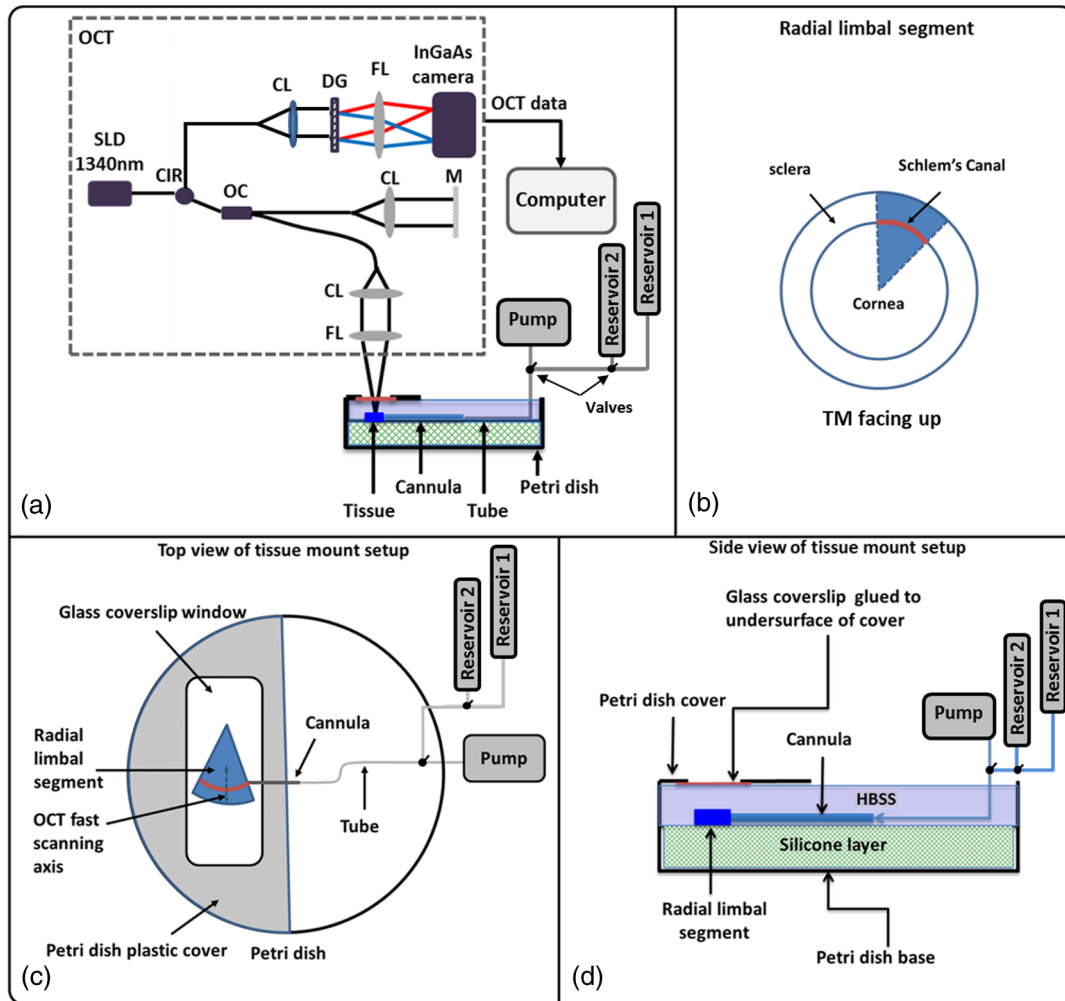


Fig. 1 (a) Schematic diagram of the experimental setup, including the spectral domain optical coherence tomography (OCT) system (dashed box), the perfusion pump used to induce pressure transients, two reservoirs used for controlling pressure in Schlemm's canal (SC), the tissue mounting arrangement, and the setup that provides a glass interface rather than a fluid interface above the specimen. (b) Schematic representation of a radial limbal segment from a corneoscleral region of the anterior segment, which is placed with the trabecular meshwork (TM) facing up. A red band depicts the position of SC. (c) and (d) show schematic diagrams of top (c) and side (d) views of the tissue mount setup in a modified Petri dish. CIR, circulator; OC, optical coupler; CL, collimation lens; FL, focusing lens; DG, diffraction grating; M, mirror; HBSS, Hank's balance salt solution.

[reservoir 1 and reservoir 2 in Fig. 1(c)]. The reservoirs placed at desired elevations provide constant known pressures. Pressures can be changed rapidly between the reservoirs at different heights by a three-way valve. The pump can be isolated from the reservoirs to deliver various combinations of flow rates and volumes.

2.2 Tissue Preparation

NHP enucleated eyes, macaca nemestrina (3), macaca mullata (1) eyes, were provided by the University of Washington Primate Center and obtained within 0.5 h of initiation of the experiments (age: mean 10.6 years, range 6.4 to 14.4 years; sex: three female, one male; weight: mean 8.7 kg, range 6.7 to 12.4 kg). The limbal region of the anterior segment containing the AOS is divided into eight equal-sized radial segments each encompassing ~45 deg of the limbal circumference [Fig. 1(b)].

The setup uses a custom-made tissue mounting arrangement designed and built as shown in Figs. 1(c) and 1(d). The setup is composed of a Petri dish covered with a silicon layer. A window is cut in the Petri dish lid and a 0.17-mm glass coverslip is mounted on the under surface. Rather than an air-water interface, the arrangement provides a uniform and stable surface during various fluid infusions, which is essential to eliminate the surface motion artifact when dynamic imaging of TM motion is performed.³¹ Silicone material, covering the bottom third of the Petri dish, permits mounting the segments with pins. The Petri dish is filled to the level of the mounted glass plate with Hank's balanced salt solution. The tissue is then mounted with the TM surface facing the imaging probe. Figures 1(c) and 1(d) show the details of the top and side views of the tissue mount setup.

Scanning electron microscopy (SEM) was used to image radial sections cut to a thickness of ~100 μm from each quadrant of the limbus of a 13.9-year-old, 6.7-kg nemestrina monkey.

Following viscoelastic SC dilation by a previously described technique,³² the sections were fixed with Karnovsky's solution. Further processing involved dehydration with graded alcohols and then postfixation with osmium, tannic acid, and uranyl acetate. After critical point drying, sections were sputtered with 6 nm of gold and palladium. The prepared segments were finally examined with SEM with efforts to obtain different tilt and rotation angles to fully characterize structural relationships. We note that SEM involves complex processing that can cause structural changes in the sample, which is a limitation of the technique. However, to gain an understanding of overall 3-D topographic relationships for comparison with 3-D SD-OCT images, the technique is useful.

2.3 Data Acquisition and Analysis of OCT Images

To evaluate the structural and dynamic pressure-dependent motion of the TM and SC regions, 3-D and MB-scan imaging modes were used. For the 3-D data acquisition, an $\sim 2 \text{ mm} \times 2 \text{ mm}$ area was scanned containing 1500 B-scans with each B-scan composed of 360 A-lines and 512 axial pixels. Acquisition was at the line rate of 92 KHz (200 frames/s). The scanning protocol was designed to acquire five B-scans at each location for improving the image contrast through averaging. To investigate the tissue responses to the change of pressure in SC, 1500 B-scans (with 360 A-lines) were acquired at the same location (MB-scan) over a 7-s time interval.

For 3-D visualization of the SC structural relationships, an algorithm was developed that binarized OCT images using a set threshold. The algorithm permitted identifying and segmenting structures with low reflectivity within the region of interest in each B-scan of the imaged tissue.³³ The resulting two-dimensional (2-D) cross-sections of the segmented SC were then assembled to generate the 3-D volumetric image of SC.

To quantify the SC area at different pressures, manual segmentation was implemented using FIJI (ImageJ software) as a means of resolving the relatively low reflectivity of SC lumen. Following manual segmentation, the software permitted delineating the SC lumen borders, thereby providing a means of segmenting SC in 2-D OCT B-scans. One-way analyses of variance (ANOVAs) were performed on the values acquired along the limbal segment at different induced pressures to permit statistical analysis of the results. Tukey multiple comparison tests were used to decide whether changes between pairs achieved a level of significance of $p < 0.05$ or better.

To quantify the TM tissue's dynamic responses to the controlled fluid infusion into SC, FIJI (ImageJ software) was used to manually measure the height and area of the SC and CCO lumens; the changing dimensions of cylindrical attachment structures (CAS) between SC walls were also assessed. To reduce the manual segmentation error, each image was quantified three times at different sessions and the mean and standard deviation of the measurements was used to generate graphs. The anatomic relationships and motion of the AOS described below are representative of the findings in each of the four eyes.

3 Results

To determine whether motion caused by rapid pulse transients could be identified and characterized, pulse transients were introduced into SC from the cannula. In Fig. 2(a), the 2-D OCT image shows the cannula inside the SC (solid arrow). The solid red arrow in Fig. 2(b) indicates the position of SC when no perfusion pressure is present in the cannula. The B-

scan location in this image is $\sim 150 \mu\text{m}$ away from the distal edge of the cannula. The beams of individual trabecular lamellae can be seen above SC as indicated by the dashed arrow. Figure 2(c) results from the introduction of a pulse transient into SC by the perfusion pump while continuously imaging using the MB-scan mode of the OCT system. The pump setting to induce the pulse transient was 30 ml/min with a set, pump-limited infusion volume of 300 μl .

Figure 2(c) is acquired at an identical location as in Fig. 2(b) and is chosen from the MB image sequence (see Video 1) at a time when SC (solid red arrow) is at its maximum dilation. At this time point, the TM is also distended and individual beams of trabecular lamellae are clearly visible (dashed arrow). A smaller region outlined by the red box in Fig. 2(c) is zoomed in Fig. 2(c) to appreciate the increased structural detail. Figure 2(d) is a representative SEM image acquired from the limbal region at a collector channel entrance or ostia (CCO). A long collagen septum or flap is visible that is parallel to the CCO and is hinged, supported only at the external wall end. Because the end protruding into the SC is unanchored, it is free to move. CAS are visible that attach to both the TM and the hinged septum at the CCO. Another hinged septum separates SC from the more distal collector channel. In the SEM image of Fig. 2(e), arrows point to different structural features, such as the collector channel and a septum dividing the lumen of SC into a compartment separate from the lumen of the collector channel entrance. Cylindrical attachments pass from the TM across SC radially to the collector channel septum along the SC external wall. Anatomic structures comparable to those identified by SEM in Fig. 2(e) are seen in the $2\times$ enlarged OCT image of the limbal region in Fig. 2(f). A septum is visible separating SC from a collector channel. CAS span between the TM and the septum, separating SC from the CC. The physical CAS connections suggest that pressure-induced TM motion would necessarily also induce motion of the septa at the CCO and the CC, leading to the changes in their respective lumen dimensions.

To determine whether structural relationships within the entire length of the lumen of SC in an individual segment could be visualized, the infusion cannula in SC was attached to a reservoir that maintained a constant infusion pressure of 50 mm Hg. Tissue from the entire length of SC was imaged along the length of the segment. Both 3-D volumetric and 2-D cross-sections were reconstructed and are shown in Fig. 3. Figure 3(a) is a side view from the edge of a radial segment where the cannula enters the SC. The tissue with the iris to the left and cornea to the right is shown in orange color. The cannula, penetrating into the canal, is shown in green, as denoted by the red arrow. A cross-section of the canal is visible at the far end of the 3-D volume, as identified by the black arrow in Fig. 3(a). Figure 3(b) is a bottom view of the same 3-D scan with the cannula in green identified by the red arrow.

Five 3-D image sets with $\sim 50\%$ overlap were acquired along the canal ($\sim 6.5 \text{ mm}$ limbal circumference) and used to create cross-sections of the SC structure. The sections were stitched together to visualize the entire canal in one radial cut of the limbal segment [Figs. 3(c) and 3(d)]. Figure 3(c) is a side view (vertical) cross-section (stitched) showing the cannula entering the lumen of SC from the right. The canal is clearly dilated throughout its length. The TM is located above the canal and is visible only in the left half of this image. A top view (horizontal) cross-section of the radial segment is shown in Fig. 3(d) that more clearly depicts the internal structures within the dilated SC.

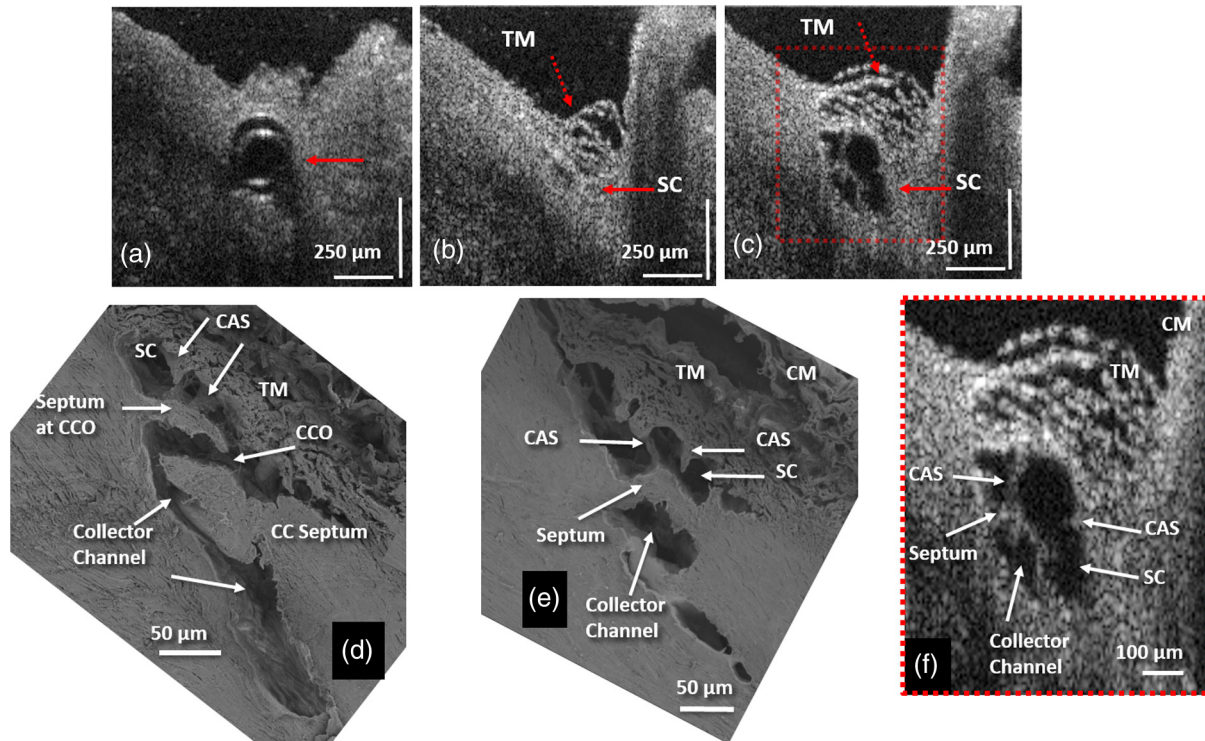


Fig. 2 Representative two-dimensional (2-D) structural OCT and scanning electron microscopy (SEM) images from the limbal region of an eye. (a) shows the OCT image captured with the cannula inside SC (arrow). At the location $\sim 150 \mu\text{m}$ away from the cannula tip, (b) shows the tissue before infusion of perfusate where arrows identify the TM and SC, while (c) shows the maximally dilated appearance of the same segment. Please also see Video 1 (MOV, 3.63 MB) [URL: <http://dx.doi.org/10.1117/1.JBO.19.10.106013.1>]. (d) and (e) are representative SEM images from the limbal region, illustrating structural features of the outflow system that are mirrored in both the SEM and OCT images. Original SEM images: 337 \times magnification. (d) shows a collector channel entrance or ostia (CCO). A septum is present at the CCO that is attached to the TM by cylindrical attachment structures (CAS). (e) is the adjacent section from the same segment showing the transition from the region of a CCO in (d) to a circumferentially oriented collector channel. (f) The 2 \times enlargement OCT image that is cropped from (c) permits a more detailed comparison of relationships. CM, ciliary muscle.

The cannula cannot be seen in Fig. 3(d) due to its oblique angle of insertion relative to the image plane. The red arrow, however, shows its location. The canal appears to discontinue at the left and right ends of the segment in Fig. 3(d) due to the limbal curvature, resulting in local elevation of the tissue relative to the image plane.

The highly reflective structures inside SC [star-marked in Fig. 3(d)] are cross-sections of the internal features of septa, which are oriented parallel to SC lumen. The septa separate SC lumen from the lumen of the circumferentially oriented collector channels that also course parallel to SC before passing upward into the sclera [blue arrows in Fig. 3(d)]. Serial images reveal CAS spanning from the TM to the SC external wall area (yellow arrows). CAS are oriented perpendicularly or obliquely to the SC circumference with attachments to both the TM and to the septa along SC external wall. Several collector channel entrances are seen between the parallel highly reflective septa, giving the septa a perforated appearance. Collector channel entrances oriented perpendicularly [green arrows in Fig. 3(d)] or obliquely (purple arrow) to SC lumen connect SC to the circumferentially oriented intrascleral collector channels.

The dilated SC structure can also be visualized by segmenting the canal at the lumen border and then setting a threshold and binarizing each OCT B-scan to extract the volume of the

minimally reflective SC as shown in Fig. 4(a). The red box in the image shows the region of interest, and the subset image [Fig. 4(a), bottom left] shows the extracted SC cross-section with inverted contrast. To produce a 3-D view of the dilated canal, 300-segmented SC cross-sections were assembled in a stack. Cross-sections included a 2-mm-long radial image set at the center of the 6.5-mm-long circumferential segment. Figure 4(b) shows a representative side view of the 3-D reconstructed SC. Various SC shapes and internal structural features can be seen at selected locations along the circumference of SC as depicted in Figs. 4(c) to 4(f).

To quantify changes in SC lumen size in response to changes in pressure within its lumen, the same limbal location was imaged at different pressures: 10, 20, 30, 40, and 50 mm Hg. Pressures were controlled by altering the heights of the reservoir attached to the cannula inserted into SC lumen. The canal area was measured at 10 equally spaced locations (i.e., every $100 \mu\text{m}$) along a 1 mm length of the limbal segment. The margins of SC lumen were manually delineated and the area then quantified using FIJI (ImageJ software). Figures 5(a), 5(b), and 5(c) show representative OCT images acquired from a single location in the canal at pressures of 10, 30, and 50 mm Hg, respectively. A progressive pressure-dependent increase in dilation of the canal lumen is clearly observed in these images.

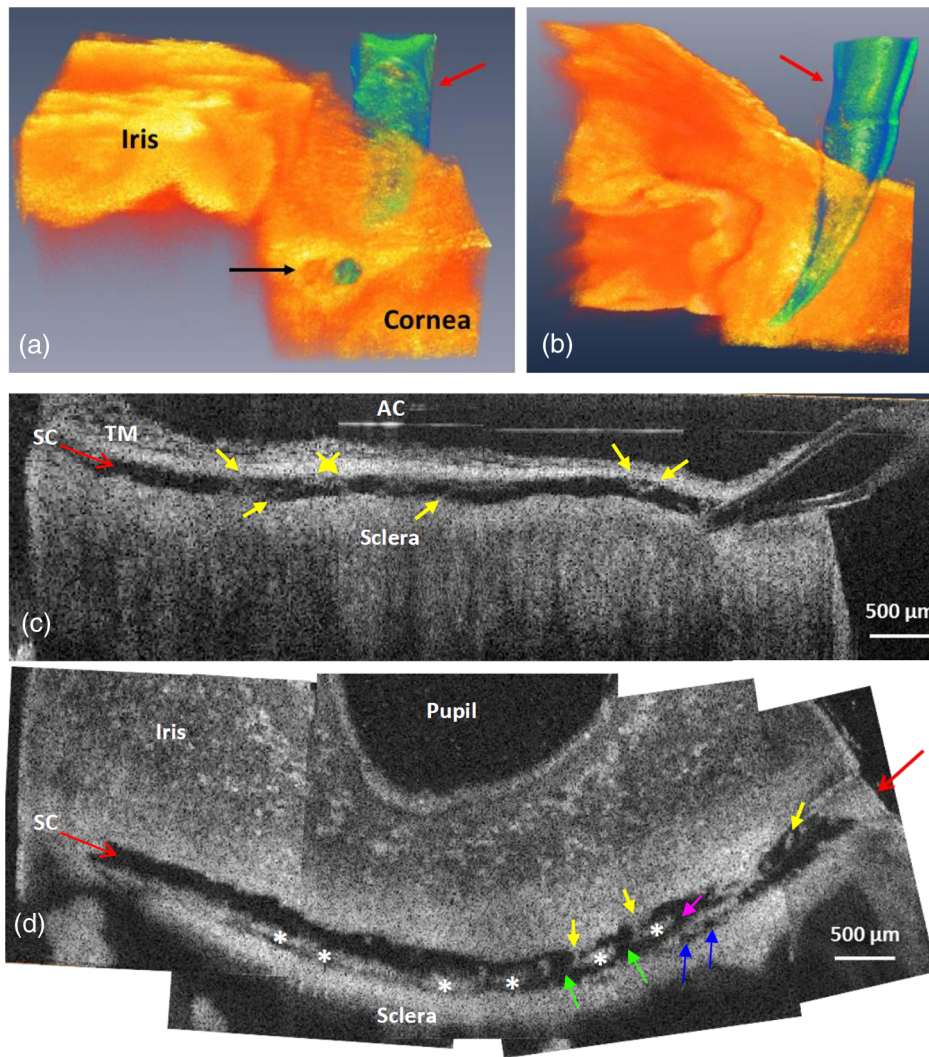


Fig. 3 Representative 3-D reconstruction of the limbal tissue. (a) is a side view of the 3-D structure of the corneo-scleral limbus where the cannula is shown in green color entering the lumen of SC, and the black arrow identifies the cross-section of the canal. (b) is a bottom view of the same 3-D limbal region. (c) is a tangential section of SC over the entire length of limbal segment, obtained from stitching five overlapping 3-D scans. (d) is a section of SC obtained from a plane oriented perpendicularly to the canal circumference. Yellow arrows in (c) and (d) identify cylindrical attachment structures spanning between the walls of SC. Purple and green arrows: CCO. Blue arrows in (d) show entrances of intrascleral collector channels. Star marks: septa that divide SC from circumferentially oriented collector channels paralleling SC.

Figure 5(d) provides a statistical analysis of the area measurements along the canal in this segment. When compared to that of the 10 mm Hg baseline pressure, the mean SC area was increased by $\sim 36\%$ at 20 mm Hg, $\sim 60\%$ at 30 mm Hg, $\sim 70\%$ at 40 mm Hg, and $\sim 90\%$ at 50 mm Hg. Statistical analysis of the canal area was made using one-way ANOVA and Tukey paired comparison tests. Significant differences in the canal area were found when comparing (1) 10 and 30 mm Hg ($P = 9.33163E - 4$), (2) 10 and 40 mm Hg ($P = 1.39769E - 4$), (3) 10 and 50 mm Hg ($P = 3.23618E - 6$), and (4) 20 and 50 mm Hg ($P = 0.0051$). The obvious change in lumen size between 10 and 30 mm Hg contrasted with little change between 30 and 50 mm Hg. Our future studies will focus on assessment of pressures between 10 and 30 mm Hg.

To determine whether quantification of the AOS tissue's dynamic responses is possible, we created a pulse transient

and monitored the tissue responses. Pulse transient creation was achieved by introducing a total 300 μL fluid volume at a 30 mL/min flow rate into SC with a Harvard Perfusion PumpTM. The canal region was simultaneously imaged using the MB-scan mode of the OCT over a 700 ms interval. Several parameters, including the SC, CC, and CAS height as well as SC and CC area, were measured manually using FIJI (ImageJ software). Figure 6(a) is the same OCT B-scan as in Fig. 2(c), which is a representative image acquired during the pulsed infusion into the canal. Different features are delineated with colored lines as well as numbers: (1) SC area (yellow line), (2) CC area (green line), (3) SC height (purple line), (4) CAS height (red line), and (5) CC height (blue line).

Figure 6(b) shows the SC, CC, and CAS heights over time in black, red, and blue, respectively. The SC and CC areas are shown in Figs. 6(c) and 6(d), respectively. As seen from all

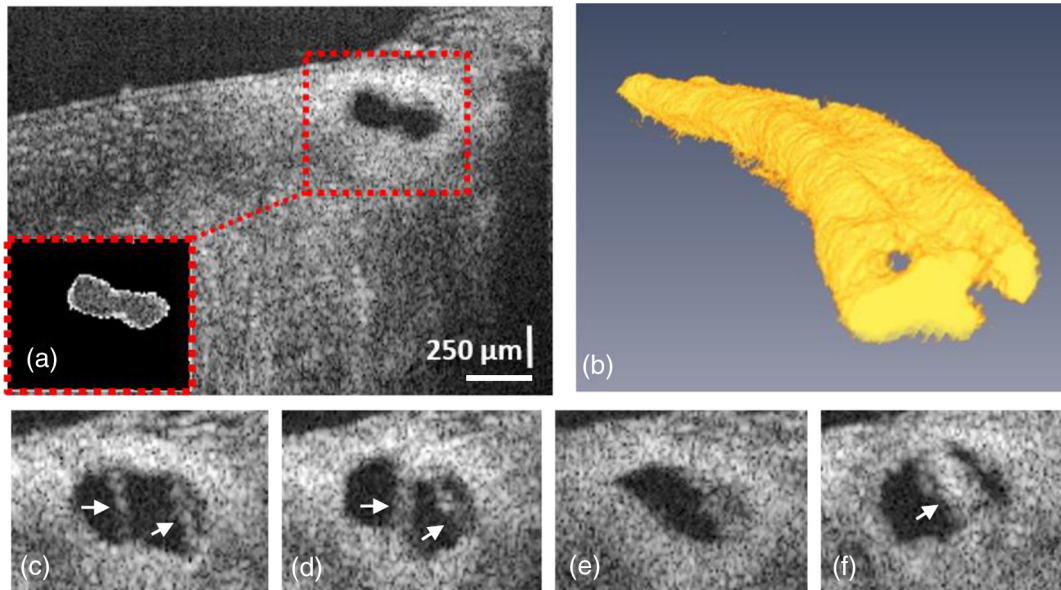


Fig. 4 (a) A representative B-scan with the region of interest, containing SC (red box), and the segmented SC from the same B-scan is shown in the inset. (b) Side view of the reconstructed 3-D SC. (c) to (f) Selected cross-sections from the SC showing its various shapes along a 2 mm length of a limbal segment. White arrows indicate locations of cylindrical attachment structures spanning between the TM and SC external wall.

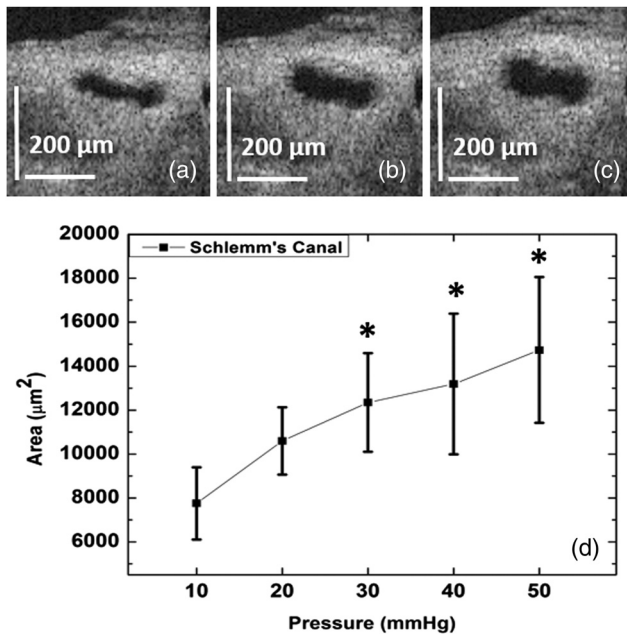


Fig. 5 Representative 2-D OCT cross-sections from the same location along SC in a radial segment of a monkey eye showing the canal at different pressures of (a) 10, (b) 30, and (c) 50 mm Hg. Measurements were performed for five pressures of 10, 20, 30, 40, and 50 mm Hg at the same location. (d) The average and standard deviation of SC cross-sectional area acquired from 10 equally spaced locations inside the canal lumen along a 1-mm-long tissue segment at 10, 20, 30, 40, or 50 mm Hg pressure. Asterisks in (d) indicate the significant change of the canal area compared to the 10 mm Hg ($n = 10$). Note that the number 10 is the number of samples along the 1 mm SC segment that was imaged at different pressures, i.e., at each pressure the SC area was measured at 10 equally spaced locations (~100 μm apart), and these 10 values were used to determine the mean and STD of SC area at each pressure.

the curves measured, the canal is closed before the infusion and, hence, the value is zero for the heights at $t = 0$. The values increase rapidly over time and begin to plateau at ~150 to 300 ms after the start of infusion. To reduce the human error associated with manual segmentation, each image was quantified three times for each of the five parameters (two areas and three heights); means and standard deviations were then used to plot the graphs. To quantify the mean dilation velocity of canal lumen dimension changes, the rate of the canal height change over time was calculated ($\Delta\text{Height}/\Delta t$) and plotted in Fig. 6(e) for SC and in Fig. 6(f) for CC. The highest mean velocity of the SC lumen change is (~1.47 mm/s) at the initial phase of the dilation and drops rapidly, reduced by an order of magnitude at later time points. In the case of the CC, the highest mean velocity is also at the beginning of the dilation (~0.43 mm/s) and decreases rapidly over time.

4 Discussion

This pilot study was aimed at assessing the technical capabilities of a new experimental prototype system incorporating SD-OCT to image the AOS in NHP eyes. The results obtained from this study indicate that the proposed integrated system allows OCT at an improved resolution to characterize and quantitatively image the TM and SC lumen, as well as the surrounding and internal structures. The imaging findings also provide an indication that the quantitation of rapid pressure-dependent motion of the TM, structures within SC, and the region of CCO is feasible as are the changes in collector channel lumen dimensions.

The proposed setup introduced a new approach for imaging the anatomy of the AOS and its responses to rapid changes in pressure gradients by using fresh tissue from NHP eyes. The system images the AOS from the TM surface, while using controlled pressures and introduction of a fluid pulse waves into SC, a combination of methods that has not been reported previously. We have shown that the system allows OCT to visualize the

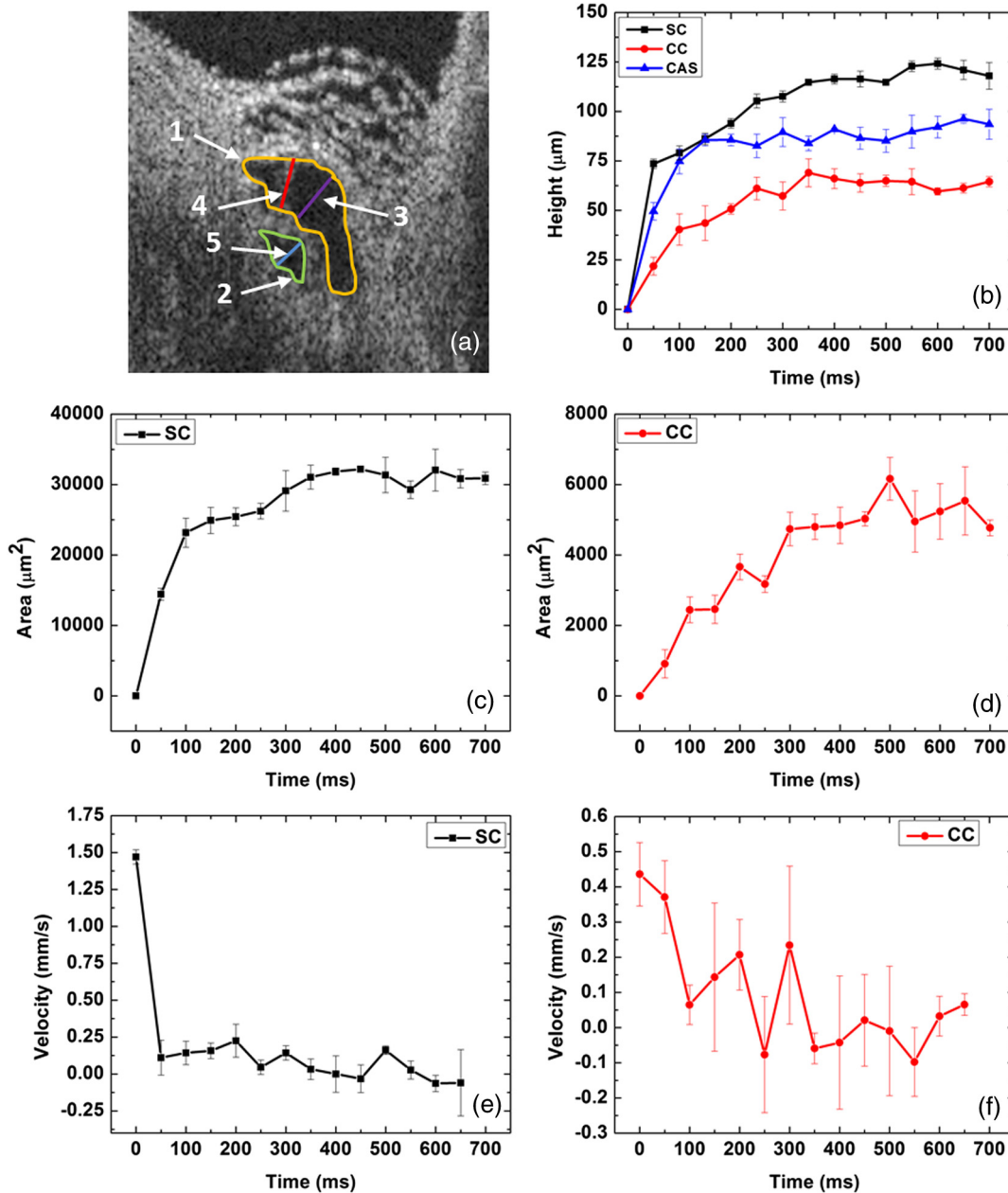


Fig. 6 (a) Representative 2-D OCT image of SC and its adjacent collector channel at its dilation maximum after a pulsed infusion, where parameters for quantification are shown: SC height, purple line; CC height, blue line; CAS height, red line; SC area, yellow line; CC area, green line. (b) Progressive increase in the height of SC (black curve), CC (red curve), and CAS (blue curve). (c) The change in SC lumen area. (d) The change in CC lumen area. (e) The change in the mean velocity of SC lumen height. (f) The change in the velocity of CC lumen height.

detailed internal structures of SC and CC. Images are of sufficient resolution for identifying the features within SC and CC region with detail similar to SEM images, an imaging capability not previously achievable with fresh ocular tissue. With the demonstrated imaging ability of the system, the 3-D structure of the lumen of SC and structural elements in the canal can be reconstructed under conditions of SC dilation by known pressures. Movement of the AOS structures can also be captured at a millisecond time resolution by a means of pulsed infusions. Although the current study was limited to NHP eyes, experiments involving postmortem human eyes are valuable and are the subject of an ongoing current study.

We attribute the enhanced measurement capabilities to (1) imaging of the outflow system from the TM (AC) surface rather than the scleral surface, (2) reversal of pressure gradients across the TM to dilate SC, which makes the assessment of structural relationships in SC and at CC entrances feasible, (3) *ex vivo* preparation to avoid motion artifact, permitting repeated measurements to be made at the same site that enables the averaging of image information, (4) a lack of motion further permitting parameters such as IOP and pulsed infusion to be done with the assurance that the measurement of different parameters can be compared from the same site, (5) an increase in resolution because the *ex vivo* arrangement permits the OCT to place its

focal plane much closer to the tissue than can be practically done *in vivo*, and (6) the use of a coverslip to couple the fluid surface to the glass that avoids the reduction of image quality associated with an air–fluid interface. The combination of these factors provides high resolution and high image contrast, allowing clear visualization, precise segmentation, and quantification of both tissue structure and motion.

A particular advantage of the current study is the ability to provide the condition of the reversal of pressure gradients across the TM, closely paralleling the methods used in clinical studies to identify abnormal outflow system responses in glaucoma.^{34–38} Physiologic positions, such as those commonly occurring in physical fitness activities, can cause pressure reversal with pressure in SC being higher than IOP.³⁹ During the physical activities involving body inversion, episcleral venous pressure rapidly rises. Increased episcleral venous pressure is necessarily reflected in an increase in SC pressure, causing a pressure reversal across the TM. Under this circumstance, blood is observed to enter SC.⁴⁰ Aqueous cannot flow against the pressure gradient in SC and a highly significant correlation has been found between the episcleral venous pressure and the IOP rise.⁴⁰ Two prior studies reported an IOP increase within seconds from the mid-teens to mid-30s following the inversion.^{39,41}

Various clinical diagnostic techniques intentionally induce SC pressure to be higher than IOP. In this case, because the TM is transparent, the SC blood reflux phenomenon is directly observable in human subjects. In mild glaucoma, when pressure gradients are reversed, the rate of speed of blood influx into SC begins to slow. As the glaucoma process advances, SC blood influx progressively slows. In the later stages of the disease, some regions of the canal no longer fill with blood, while in far advanced disease, no SC blood filling is observed.^{34–38} Altered blood reflux into SC represents the only directly observable abnormality of the TM and SC regions in glaucoma.

The findings of the lack of SC blood filling in glaucoma patients have been interpreted as representing a progressive loss of the ability of the trabecular tissues to undergo motion that normally permits enlargement of SC in response to pressure gradient changes. Motion of the TM as well as maintenance of the optimal SC lumen size is dependent on the compliance and elasticity of the TM tissues. These tissue properties have eluded study until now because appropriate experimental techniques and related imaging technology have not been available.

SC pressure reversal and lumen dilation by cannulation has been extensively used clinically as a procedure to reduce IOP in glaucoma.^{34,42,43} Dilation of SC is accomplished by SC cannulation and the introduction of a high-viscous hyaluronic acid into the canal lumen. Persistent SC dilation is also used in glaucoma by tensioning a suture placed within the entire circumference of SC.⁴⁴ The effects of pressure-induced reversal have, in addition, been studied in the laboratory and shown to cause marked changes in SC structural relationships.³² Devices currently being inserted into SC in the operating room to bypass the TM are thought to achieve their best effect when placed near CCO; at the same time, efforts are made to avoid damage to or occlusion of CCO. The positioning of MIGS devices has been evaluated through imaging with SEM,^{45,46} but not OCT. Device placement requirements illustrate the need for *in vivo* imaging tools to inform device development and to optimize device placement, thereby enabling improvement of clinical outcomes.

A noteworthy study recently demonstrated an ability to use an endoscopic approach to image collector channels in an *ex vivo* human eye with a swept source OCT contained within an endoscopic probe.²⁹ The study raised the possibility of using such an approach clinically to identify collector channels for the purposes of more precise SC device placement. The probe imaged the AOS from the TM surface as was done in the current study. In their initial prototype, limitations included data acquisition at a frame rate of 0.5 fps in contrast to the 200 fps in our study.

The high resolution and ability to detect motion illustrated by our study provides support for the concept that an improved endoscopic or catheter probe imaging through the TM surface could be a valuable tool for managing glaucoma issues. Our study further suggests that the development of optimizing algorithms for *in vivo* transscleral OCT imaging may have clinical promise. Of interest, several of the techniques used to reverse SC pressure gradients are amenable to use in conjunction with either trans-TM or transscleral OCT imaging.^{34,37,47}

Limitations of the current technique involve some of the same issues present in other *ex vivo* studies, including a lack of ciliary body tension and a lack of normal episcleral venous pressure. In our study, trans-trabecular flow into the AC from SC could be a confounding variable. However, *in vivo* studies demonstrate that the collapse of the TM prevents fluid from flowing into the AC from SC.^{26,34,37,40,47–49} Another confounding variable relates to the ability of the fluid to flow along SC from the cannula end to the other open cut end of the canal in these tissue segments. The cut open end of SC may permit rapid outflow, resulting in a progressive reduction in pressure in locations distal to the cannula end. As fluid flows along SC, it will also encounter CCO, which will also progressively divert flow along the canal circumference. Accordingly, pressure gradients determined by reservoir height can be at most equal pressure in SC, but may be less by an amount that cannot be accurately determined.

Evidence from the current study provides some insights related to these potentially confounding variables. The cross-sectional area of SC and, especially, the dimensions of the CC are small relative to the rather large fluid volumes that are introduced into the lumen of SC in our technique. Two of our study findings suggest that pressures may remain relatively stable within the confines of SC lumen. First, the ability to widely and uniformly dilate SC, not only in proximal portion near the cannula but also 6 mm distally near the canal cut end, suggests that pressure gradient across the canal can be maintained. Second, the ability to generate graded responses of the TM tissues to the increased pressure in regions distant from the cannula indicates an ability to maintain relatively stable pressure gradients along the length of SC.

A number of important questions related to the behavior of the AOS can be raised by and become possible to study as a result of the combination of image resolution and acquisition speed achievable with the current technique. First, characterization of cyclic pressure-dependent TM motion responses becomes possible with the proposed system setup. Such motion relies on tissue elasticity and compliance, properties that determine pressure-dependent SC wall relationships. Second, with this system, it becomes feasible to explore the relationship between TM and CC entrance motion that may play a role in IOP control. Such studies are currently under way in our laboratory on human eyes.

5 Conclusion

In conclusion, we have demonstrated the capability of a prototype system setup incorporating SD-OCT to image detailed internal structures and their relationships within SC. Importantly, the technique images SC from the TM surface. After cannulating SC, we introduced fluid into SC at controlled pressures and flow rates. The technique reversed pressure gradients across the TM, thereby dilating SC. Dilation enabled us to obtain detailed images of SC, cylindrical structures spanning SC, CC shape, and septa dividing SC lumen from the collector channel lumen.

We have also demonstrated the ability of the proposed system to quantify the dynamic motion of the structural elements as well as changes in SC and CC lumen dimensions. Our results show that the SC and CC tissues are capable not only of responding to pressure, but can do so within milliseconds in response to an ocular transient. The technique described in the study should be useful for characterizing functional properties in normal eyes and abnormal properties in glaucoma eyes. The study suggests that technical advances in both transscleral and endoscopic OCT would be capable of bringing new clinical insights and management approaches to the enigma of glaucoma.

Acknowledgments

This work was supported in part by research grants from the National Eye Institute (R01EY024158), the W. H. Coulter Foundation Translational Research Partnership Program, and the Office of Research Infrastructure Programs of the National Institutes of Health through Grant No. P51OD010425 through the Washington National Primate Research Center. Part of this work was conducted at the University of Washington NanoTech User Facility, a member of the NSF National Nanotechnology Infrastructure Network, and the Biology Imaging Facility at the University of Washington. The content is solely the responsibility of the authors and does not necessarily represent the official views of the grant giving bodies.

References

- H. A. Quigley and A. T. Broman, "The number of people with glaucoma worldwide in 2010 and 2020," *Br. J. Ophthalmol.* **90**(3), 262–267 (2006).
- W. M. Grant, "Further studies on facility of flow through the trabecular meshwork," *Arch. Ophthalmol.* **60**(4), 523–533 (1958).
- W. M. Grant, "Experimental aqueous perfusion in enucleated human eyes," *Arch. Ophthalmol.* **69**(6), 783–801 (1963).
- B. A. Gabelt and P. L. Kaufman, "Production and flow of aqueous humor," in *Adler's Physiology of the Eye*, P. L. Kaufman and A. Alm, Eds., pp. 274–307, Elsevier, Edinburgh (2011).
- A. Aspelund et al., "The Schlemm's canal is a VEGF-C/VEGFR-3-responsive lymphatic-like vessel," *J. Clin. Invest.* **124**(9), 3975–3986 (2014).
- D. Y. Park et al., "Lymphatic regulator PROX1 determines Schlemm canal integrity and identity," *J. Clin. Invest.* **124**(9), 3960–3974 (2014).
- M. Johnstone, E. Martin, and A. Jamil, "Pulsatile flow into the aqueous veins: manifestations in normal and glaucomatous eyes," *Exp. Eye Res.* **92**(5), 318–327 (2011).
- M. A. Johnstone, "A new model describes an aqueous outflow pump and explores causes of pump failure in glaucoma," in *Glaucoma*, F. Grehn and R. Stamper, Eds., pp. 3–34, Springer, Berlin, Heidelberg (2006).
- J. R. Levick, *Introduction to Cardiovascular Physiology*, CRC Press, Boca Raton, FL (2010).
- L. M. Brandao and M. C. Grieshaber, "Update on minimally invasive glaucoma surgery (MIGS) and new implants," *J. Ophthalmol.* **2013**, 705915 (2013).
- N. M. Radcliffe, M. G. Lynch, and R. H. Brown, "Ab interno stenting procedures," *J. Cataract Refract. Surg.* **40**(8), 1273–1280 (2014).
- A. Fercher et al., "Optical coherence tomography—principles and applications," *Rep. Prog. Phys.* **66**(2), 239 (2003).
- D. Huang et al., "Optical coherence tomography," *Science* **254**(5035), 1178–1181 (1991).
- P. H. Tomlin and R. K. Wang, "Theory, development and applications of optical coherence tomography," *J. Phys. D: Appl. Phys.* **38**(15), 2519 (2005).
- G. Li et al., "Pilocarpine-induced dilation of Schlemm's canal and prevention of lumen collapse at elevated intraocular pressures in living mice visualized by OCT," *Invest. Ophthalmol. Vis. Sci.* **55**(6), 3737–3746 (2014).
- P. Li et al., "Phase-sensitive optical coherence tomography characterization of pulse-induced trabecular meshwork displacement in *ex vivo* nonhuman primate eyes," *J. Biomed. Opt.* **17**(7), 076026 (2012).
- P. Li et al., "In vivo microstructural and microvascular imaging of the human corneo-scleral limbus using optical coherence tomography," *Biomed. Opt. Express* **2**(11), 3109–3118 (2011).
- P. Li et al., "Extended imaging depth to 12 mm for 1050-nm spectral domain optical coherence tomography for imaging the whole anterior segment of the human eye at 120-kHz A-scan rate," *J. Biomed. Opt.* **18**(1), 016012 (2013).
- P. Li et al., "Pulsatile motion of the trabecular meshwork in healthy human subjects quantified by phase-sensitive optical coherence tomography," *Biomed. Opt. Express* **4**(10), 2051–2065 (2013).
- P. Li, M. Johnstone, and R. K. Wang, "Full anterior segment biometry with extended imaging range spectral domain optical coherence tomography at 1340 nm," *J. Biomed. Opt.* **19**(4), 046013 (2014).
- M. V. Sarunic et al., "Imaging the ocular anterior segment with real-time, full-range Fourier-domain optical coherence tomography. Detailed visualization of the anterior segment using Fourier-domain optical coherence tomography," *Arch. Ophthalmol.* **126**(4), 537–542 (2008).
- G. Shi et al., "Morphometric measurement of Schlemm's canal in normal human eye using anterior segment swept source optical coherence tomography," *J. Biomed. Opt.* **17**(1), 016016 (2012).
- T. A. Tun et al., "Assessment of trabecular meshwork width using swept source optical coherence tomography," *Graefes Arch. Clin. Exp. Ophthalmol.* **251**(6), 1587–1592 (2013).
- T. Usui et al., "Identification of Schlemm's canal and its surrounding tissues by anterior segment Fourier domain optical coherence tomography," *Invest. Ophthalmol. Vis. Sci.* **52**(9), 6934–6939 (2011).
- F. Wang et al., "Comparison of Schlemm's canal's biological parameters in primary open-angle glaucoma and normal human eyes with swept source optical," *J. Biomed. Opt.* **17**(11), 116008 (2012).
- M. A. Johnstone and W. G. Grant, "Pressure-dependent changes in structures of the aqueous outflow system of human and monkey eyes," *Am. J. Ophthalmol.* **75**(3), 365–383 (1973).
- L. Kagemann et al., "IOP elevation reduces Schlemm's canal cross-sectional area," *Invest. Ophthalmol. Vis. Sci.* **55**(3), 1805–1809 (2014).
- L. Kagemann et al., "Identification and assessment of Schlemm's canal by spectral-domain optical coherence tomography," *Invest. Ophthalmol. Vis. Sci.* **51**(8), 4054–4059 (2010).
- J. Ren et al., "Ex vivo optical coherence tomography imaging of collector channels with a scanning endoscopic probe," *Invest. Ophthalmol. Vis. Sci.* **52**(7), 3921–3925 (2011).
- I. Grierson and W. R. Lee, "The fine structure of the trabecular meshwork at graded levels of intraocular pressure. (1) Pressure effects within the near-physiological range (8–30 mmHg)," *Exp. Eye Res.* **20**(6), 505–521 (1975).
- S. Song, Z. Huang, and R. K. Wang, "Tracking mechanical wave propagation within tissue using phase-sensitive optical coherence tomography: motion artifact and its compensation," *J. Biomed. Opt.* **18**(12), 121505 (2013).
- B. A. Smit and M. A. Johnstone, "Effects of viscoelastic injection into Schlemm's canal in primate and human eyes: potential relevance to viscocanalostomy," *Ophthalmology* **109**(4), 786–792 (2002).

33. X. Yin, J. R. Chao, and R. K. Wang, "User-guided segmentation for volumetric retinal optical coherence tomography images," *J. Biomed. Opt.* **19**(8), 086020 (2014).
34. M. C. Grieshaber et al., "Clinical evaluation of the aqueous outflow system in primary open-angle glaucoma for canaloplasty," *Invest. Ophthalmol. Vis. Sci.* **51**(3), 1498–1504 (2010).
35. K. E. Schirmer, "Gonioscopic assessment of blood in Schlemm's canal. Correlation with glaucoma tests," *Arch. Ophthalmol.* **85**(3), 263–267 (1971).
36. K. E. Schirmer, "Reflux of blood in the canal of Schlemm, quantitated," *Can. J. Ophthalmol.* **4**(1), 40–44 (1969).
37. E. B. Suson and R. O. Schultz, "Blood in Schlemm's canal in glaucoma suspects. A study of the relationship between blood-filling pattern and outflow facility in ocular hypertension," *Arch. Ophthalmol.* **81**(6), 808–812 (1969).
38. P. C. Kronfeld, "Further gonioscopic studies on the canal of Schlemm," *Arch. Ophthalmol.* **41**(4), 393 (1949).
39. R. N. Weinreb, J. Cook, and T. R. Friberg, "Effect of inverted body position on intraocular pressure," *Am. J. Ophthalmol.* **98**(6), 784–787 (1984).
40. T. R. Friberg, G. Sanborn, and R. N. Weinreb, "Intraocular and episcleral venous pressure increase during inverted posture," *Am. J. Ophthalmol.* **103**(4), 523–526 (1987).
41. T. R. Friberg and R. N. Weinreb, "Ocular manifestations of gravity inversion," *JAMA* **253**(12), 1755–1757 (1985).
42. M. C. Grieshaber et al., "Canaloplasty for primary open-angle glaucoma: long-term outcome," *Br. J. Ophthalmol.* **94**(11), 1478–1482 (2010).
43. R. Stegmann, A. Pienaar, and D. Miller, "Viscocanalostomy for open-angle glaucoma in black African patients," *J. Cataract Refract. Surg.* **25**(3), 316–322 (1999).
44. M. C. Grieshaber et al., "Comparing two tensioning suture sizes for 360 degrees viscocanalostomy (canaloplasty): a randomised controlled trial," *Eye (Lond)* **24**(7), 1220–1226 (2010).
45. C. K. Bahler et al., "Second-generation trabecular meshwork bypass stent (iStent inject) increases outflow facility in cultured human anterior segments," *Am. J. Ophthalmol.* **153**(6), 1206–1213 (2012).
46. M. A. Johnstone, H. Saheb, and I. I. K. Ahmed, "Effects of a Schlemm canal scaffold on collector channel ostia in human anterior segments," *Exp. Eye Res.* **119**(2), 70–76 (2014).
47. P. C. Kronfeld, H. T. McGarry, and H. E. Smith, "Gonioscopic study on the canal of Schlemm," *Am. J. Ophthalmol.* **25**(10), 1163 (1942).
48. I. Grierson and W. R. Lee, "The fine structure of the trabecular meshwork at graded levels of intraocular pressure. (2) Pressures outside the physiological range (0 and 50 mmHg)," *Exp. Eye Res.* **20**(6), 523–530 (1975).
49. J. E. Pederson, H. M. MacLellan, and D. E. Gaasterland, "The rate of reflux fluid movement into the eye from Schlemm's canal during hypotony in the rhesus monkey," *Invest. Ophthalmol. Vis. Sci.* **17**(4), 377–381 (1978).

Biographies of the authors are not available.